
QUANTILE-LSTM: A ROBUST LSTM FOR ANOMALY DETECTION IN TIME SERIES DATA

Snehanshu Saha

Department of CSIS and APPCAIR
Birla Institute of Technology and Science
Goa, India
snehanshus@goa.bits-pilani.ac.in

Jyotirmoy Sarkar

Department of CSIS
Birla Institute of Technology and Science
Goa, India
jyotirmoy208@gmail.com

Soma Dhavala

Founder
MLSquare
Bengaluru, India
soma@mlsquare.org

Santonu Sarkar

Department of CSIS
Birla Institute of Technology and Science
Goa, India
santonus@gmail.com

Preyank Mota

Department of CSIS
Birla Institute of Technology and Science
Goa, India
f20190331@goa.bits-pilani.ac.in

ABSTRACT

Anomalies refer to the departure of systems and devices from their normal behaviour in standard operating conditions. An anomaly in an industrial device can indicate an upcoming failure, often in the temporal direction. In this paper, we make two contributions: 1) we estimate conditional quantiles and consider three different ways to define anomalies based on the estimated quantiles. 2) we use a new learnable activation function in the popular Long Short Term Memory networks (LSTM) architecture to model temporal long-range dependency. In particular, we propose Parametric Elliot Function (PEF) as an activation function (AF) inside LSTM, which saturates lately compared to *sigmoid* and *tanh*. The proposed algorithms are compared with other well-known anomaly detection algorithms, such as Isolation Forest (iForest), Elliptic Envelope, Autoencoder, and modern Deep Learning models such as Deep Autoencoding Gaussian Mixture Model (DAGMM), Generative Adversarial Networks (GAN). The algorithms are evaluated in terms of various performance metrics, such as Precision and Recall. The algorithms have been tested on multiple industrial time-series datasets such as Yahoo, AWS, GE, and machine sensors. We have found that the LSTM-based quantile algorithms are very effective and outperformed the existing algorithms in identifying anomalies.

1 Introduction

Anomalies indicate a departure of a system from its normal behaviour. In Industrial systems, they often lead to failures. By definition, anomalies are rare events. As a result, from a Machine Learning standpoint, collecting and classifying anomalies pose significant challenges. For example, when anomaly detection is posed as a classification problem, it leads to extreme class imbalance (data paucity problem). Though several current approaches use semi-supervised neural network to detect anomalies [11, 19], these approaches still require some labeled data. In the recent past, there have been approaches that attempt to model normal dataset and consider any deviation from the normal as an anomaly. For instance, autoencoder-based family of models [6] use some form of thresholds to detect anomalies. Another class of approaches relied on reconstruction errors [17], as an anomaly score. If the reconstruction error of a datapoint is higher than a threshold, then the datapoint is declared as an anomaly. However, the threshold value can be specific to the domain and the model, and deciding the threshold on the reconstruction error can be cumbersome.

In this paper, we have introduced the notion of *quantiles* in multiple versions of the LSTM-based anomaly detector. Our proposed approach is principled on:

- training models on a normal dataset
- modeling temporal dependency

- proposing an adaptive solution that does not require manual tuning of the activation

Since our proposed model tries to capture the normal behavior of an industrial device, it does not require any expensive dataset labeling. Our approach also does not require re-tuning of threshold values across multiple domains and datasets. We have exhibited through empirical results later in the paper (see Table 11 of Appendix E) that the distributional variance does not impact the prediction quality. Our contributions are three folds:

- (1) Introduction of *quantiles*, free from the assumptions on data distributions, in design of quantile-based LSTM techniques and their application in anomaly identification.
- (2) Proposal of the *Parameterized Elliot* as a 'flexible-form, adaptive, learnable' activation function in LSTM, where the parameter is learned from the dataset. Therefore, it does not require any manual retuning when the nature of the dataset changes. We have shown empirically that the modified LSTM architecture with PEF performed better than the Elliot Function (EF) and showed that such behavior might be attributed to the slower saturation rate of PEF.
- (3) Demonstration of *superior performance* of the proposed LSTM methods over state-of-the-art (SoTA) deep learning (Autoencoder [24], DAGMM [27], DevNet [14]) and non-deep learning algorithms (iForest [9], Elliptic envelope [15])

The rest of the paper is organized as follows. The proposal and discussion of various LSTM-based algorithms are presented in section 2. Section 3 describes the LSTM structure and introduces the PEF. This section also explains the intuition behind choosing a parameterized version of the AF and better variability due to it. Experimental results are presented in section 4. Section 5 discusses relevant literature in anomaly detection. We conclude the paper in section 6.

2 Anomaly detection with Quantile LSTMs

Since *distribution independent* and *domain independent* anomaly detection are the two key motivation behind this work, we borrow the concept of quantiles from Descriptive and Inferential Statistics to address this challenge.

2.1 Why Quantile based approach?

Quantiles are used as a robust alternative to classical conditional means in Econometrics and Statistics [8]. In a previous work, Tambwekar et.al.[21] extended the notion of conditional quantiles to the binary classification setting, allowing to quantify the uncertainty in the predictions and provide interpretations into the functions learnt by the models via a new loss called binary quantile regression loss (sBQC). The estimated quantiles are leveraged to obtain individualized confidence scores that provide an accurate measure of a prediction being misclassified. Since quantiles are a natural choice to quantify uncertainty, they are a natural candidate for anomaly detection. However, to the best of our knowledge, quantile based method has not been used for anomaly detection, however natural it seems.

Empirically, if the data being analyzed are not actually distributed according to an assumed distribution, or if there are other potential sources for anomalies that are far removed from the mean, then quantiles may be more useful descriptive statistics than means and other moment-related statistics. Quantiles can be used to identify probabilities of the range of normal data instances such that data lying outside the defined range are conveniently identified as anomalies.

The important aspect of distribution-free anomaly detection is the anomaly threshold being agnostic to the data from different domains. Simply stated, once a threshold is set (in our case, 10-90), we don't need to tune the threshold in order to detect anomalous instances for different data sets. Quantiles allows using distributions for many practical purposes, including looking for confidence intervals. Quantile divides a probability distribution into areas of equal probability i.e. quantiles offer us to quantify chances that a given parameter is inside a specified range of values. This allows us to determine the confidence level of an event (anomaly) actually occurring.

Though the mean of a distribution is a useful measure when it is symmetric, there is no guarantee that actual data distributions are symmetric. If there are potential sources for anomalies are far removed from the mean, then medians are more robust than means, particularly in skewed and heavy-tailed data. It is well known that quantiles minimize check loss [5], which is a generalized version of Mean Absolute Error (MAE) arising from medians rather than means. Thus, quantiles have less susceptibility to long-tailed distributions and outliers, in comparison to mean [3].

Therefore, it makes practical sense to investigate the power of quantiles in detecting anomalies in data distributions. Unlike the methods for anomaly detection in the literature, our proposed quantile-based thresholds applied in the quantile-LSTM are generic and not specific to the domain or dataset. The need to isolate anomalies from the underlying distribution is significant since it allows us to detect anomalies irrespective of the assumptions on the underlying data distribution. We have introduced the notion of quantiles in multiple versions of the LSTM-based anomaly detector

in this paper, namely (i) quantile-LSTM (ii) iqr-LSTM and (iii) Median-LSTM. All the LSTM versions are based on estimating the quantiles instead of the mean behaviour of an industrial device. Note, the median is 50% quantile.

2.2 Various quantile-LSTM Algorithms

Before we discuss quantile-based anomaly detection, we describe the data structure and processing setup, with some notations. Let us consider $x_i, i = 1, 2, \dots, n$ be the n time-series training datapoints. We consider $T_k = \{x_i : i = k, \dots, k + t\}$ be the set of t datapoints, and let T_k be split into w disjoint windows with each window of integer size $m = \frac{t}{w}$ and $T_k = \{T_k^1, \dots, T_k^w\}$. Here, $T_k^j = \{x_{k+m(j-1)}, \dots, x_{k+m(j)-1}\}$. In Figure 1, we show the sliding characteristics of the proposed algorithm on a hypothetical dataset, with $t = 9, m = 3$. Let $Q_\tau(D)$ be the sample quantile of the datapoints in the set D . The training data consists of, for every $T_k, X_{k,\tau} \equiv \{Q_\tau(T_k^j)\}, j = 1, \dots, w$ as predictors with $y_{k,\tau} \equiv Q_\tau(T_{k+1})$, sample quantile at a future time-step, as the label or response. Let $\hat{y}_{k,\tau}$ be the predicted value by an LSTM model.

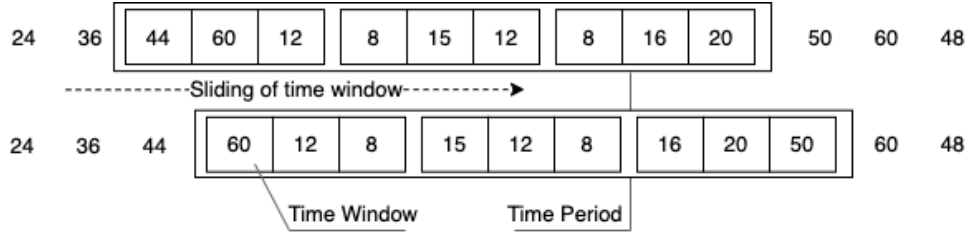


Figure 1: Sliding movement of a time period

A general recipe we are proposing to detect anomalies is to: (i) estimate quantile $Q_\tau(x_{k+t+1})$ with $\tau \in (0, 1)$ and (ii) define a statistic that measures the outlier-ness of the data, given the observation x_{k+t+1} . Instead of using global thresholds, thresholds are adaptive i.e. they change at every time-point depending on quantiles.

2.2.1 quantile-LSTM

As the name suggests, in quantile-LSTM, we forecast two quantiles q_{low} and q_{high} to detect the anomalies present in a dataset. We assume the next quantile values of the time period after sliding the time period by one position are dependent on the quantile values of the current time period.

It is further expected that, nominal range of the data can be gleaned from q_{low} and q_{high} . Using these q_{low} and q_{high} values of the current time windows, we can forecast q_{low} and q_{high} values of the next time period after sliding by one position. Here, it is required to build two LSTM models, one for q_{low} (LSTM $_{q_{low}}$) and another for q_{high} (LSTM $_{q_{high}}$). Let's take the hypothetical dataset as a training set from Figure 2a. It has three time windows from time period $x_1 \dots x_9$. Table 1 defines the three time windows of the time period $x_1 \dots x_9$ and the corresponding q_{low} , q_{high} values against the time window.

TW	q_{low}	q_{high}
x_1, x_2, x_3	$X_{1,low} \equiv Q_{low}(T_1^1)$	$X_{1,high} \equiv Q_{high}(T_1^1)$
x_4, x_5, x_6	$X_{2,low} \equiv Q_{low}(T_1^2)$	$X_{2,high} \equiv Q_{high}(T_1^2)$
x_7, x_8, x_9	$X_{3,low} \equiv Q_{low}(T_1^3)$	$X_{3,high} \equiv Q_{high}(T_1^3)$

Table 1: The first time period and its corresponding time windows

The size of the inputs to the LSTM depends on the number of time windows w and one output. Since three time windows have been considered for a time period in this example, both the LSTM models will have three inputs and one output. For example, the LSTM predicting the lower quantile, would have $X_{1,low}, X_{2,low}, X_{3,low}$ as its puts and $y_{1,low}$ as its output, for one time-period. A total of $n - t + 1$ instances will be available for training the LSTM models assuming no missing values.

After building the LSTM models, for each time period it predicts the corresponding quantile value and slides one position to the next time period on the test dataset. quantile-LSTM applies a following anomaly identification approach. If the observed value x_{k+t+1} falls outside of the predicted (q_{low}, q_{high}), then the observation will be declared as an anomaly. For example, the observed value x_{10} will be detected as an anomaly if $x_{10} < \hat{y}_{1,low}$ or $x_{10} > \hat{y}_{1,high}$. Figure 2a illustrates the anomaly identification technique of the quantile-LSTM on a hypothetical test dataset.

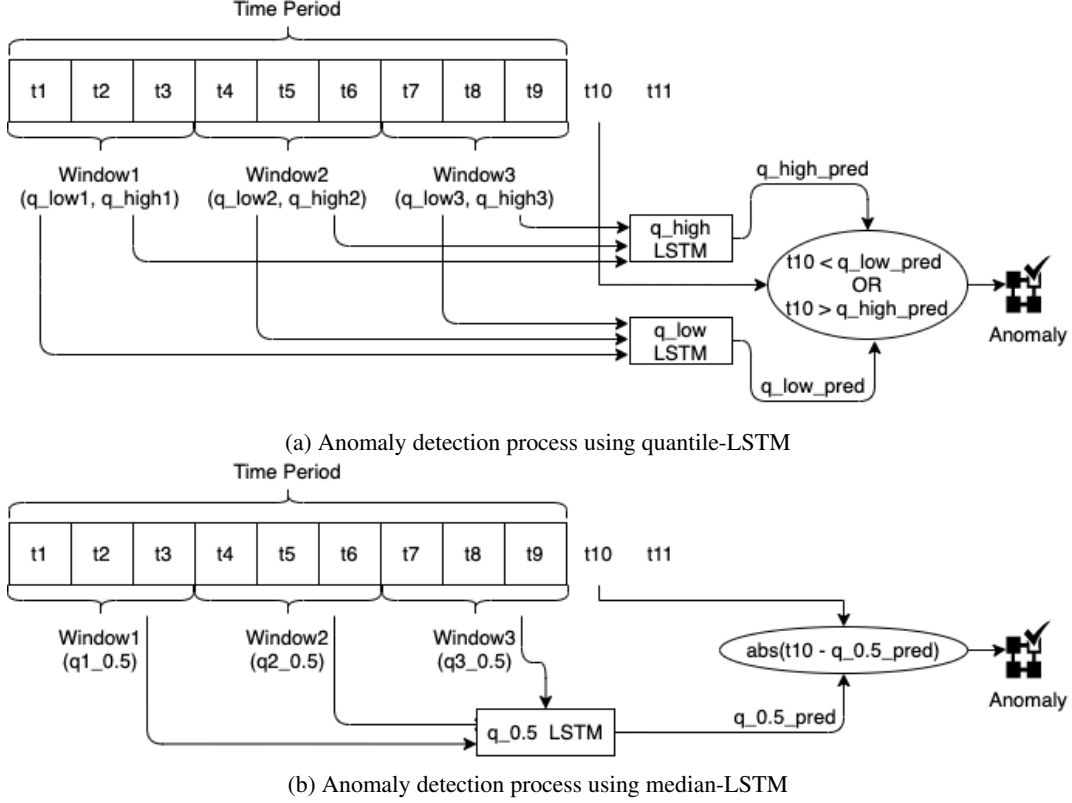


Figure 2: Sigmoid function has been applied as a recurrent function, which is applied on the outcome of the forget gate ($f_t = \sigma(W_f * [h_{t-1}, x_t] + b_f)$) as well as input gate ($i_t = \sigma(W_i * [h_{t-1}, x_t] + b_i)$). PEF decides the information to store in cell $\hat{c}_t = PEF(W_c * [h_{t-1}, x_t] + b_c)$.

2.2.2 IQR-LSTM

iqr-LSTM is a special case of quantile-LSTM where q_{low} is 0.25 and q_{high} is the 0.75 quantile. In addition, another LSTM model predicts median $q_{0.5}$ as well. Effectively, at every time index k , three predictions are made $\hat{y}_{k,0.25}, \hat{y}_{k,0.5}, \hat{y}_{k,0.75}$. Based on this, we define the Inter Quartile Range (IQR) $\hat{y}_{k,0.75} - \hat{y}_{k,0.25}$. Using IQR, the following rule identifies an anomaly when $x_{t+k+1} > \hat{y}_{k,0.5} + \alpha(\hat{y}_{k,0.75} - \hat{y}_{k,0.25})$ or $x_{t+k+1} < \hat{y}_{k,0.5} - \alpha(\hat{y}_{k,0.75} - \hat{y}_{k,0.25})$

2.2.3 Median-LSTM

Median-LSTM, unlike quantile-LSTM, does not identify the range of the normal datapoints; rather, based on a single LSTM, distance between the observed value and predicted median ($x_{t+k+1} - \hat{y}_{k,0.5}$) is computed, as depicted in Figure 2b, and running statistics are computed on this derived data stream. The training set preparation is similar to quantile-LSTM.

To detect the anomalies, Median-LSTM uses an implicit adaptive threshold. It is not reasonable to have a single threshold value for the entire time series dataset when dataset exhibits seasonality and trends. We introduce some notations to make description concrete. Adopting the same conventions introduced before, define $d_k \equiv x_{t+k+1} - Q_{0.5}(T_{k+1})$, $k = 1, 2, \dots, n-t$ and partition the difference series into s sets of size t each, i.e., $D \equiv D_p, p = 1, \dots, s$, where $D_p = \{d_i : i = (s-1)t + 1, \dots, st\}$. After computing the differences on the entire dataset, for every window D_p , mean (μ_p) and standard deviation (σ_p) for the individual time period D_p . As a result, μ_p and σ_p will differ from one time period to another time period. Median-LSTM detects the anomalies using upper threshold and lower threshold parameters of a particular time period D_p and they are computed as follows:

$$T_{p,lower} = \mu_p + w\sigma_p; T_{p,higher} = \mu_p - w\sigma_p$$

An anomaly can be flagged for $d_k \in T_p$ when either $d_k > T_{p,higher}$ or $d_k < T_{p,lower}$. Now, what should be the probable value for w ? If we consider $w = 2$, it means that any datapoint beyond two standard deviations away from the mean on either side will be considered as an anomaly. It is based on the intuition that differences of the

normal datapoints should be close to the mean value, whereas the anomalous differences will be far from the mean value. Hence 95.45% datapoints are within two standard deviations distance from the mean value. It is imperative to consider $w = 2$ since there is a higher probability of the anomalies falling into the 4.55% datapoints. We can consider $w = 3$ too where 99.7% datapoints are within three standard deviations. However, it may miss the border anomalies, which are relatively close to the normal datapoints and only can detect the prominent anomalies. Therefore we have used $w = 2$ across the experiments.

2.3 Probability Bound

In this subsection, we analyze different datasets by computing the probability of occurrence of anomalies using the quantile approach. We have considered 0.1, 0.25, 0.75, 0.9, and 0.95 quantiles and computed the probability of anomalies beyond these values, as shown in Table 10 of appendix section. The multivariate datasets are not considered since every feature may follow a different quantile threshold. Hence it is not possible to derive a single quantile threshold for all the features. It is evident from Table 10 of Appendix A of that the probability of a datapoint being an anomaly is high if the datapoint’s quantile value is either higher than 0.9 or lower than 0.1. However, if we increase the threshold to 0.95, the probability becomes 0 across the datasets. This emphasizes that a higher quantile threshold does not detect anomalies. It is required to identify the appropriate threshold value, and it is apparent from the table that most of the anomalies are nearby 0.9 and 0.1 quantile values. Table 10 also demonstrates the different nature of the anomalies present in the datasets. For instance, the anomalies of Yahoo Dataset₁ to Yahoo Dataset₆ are present nearby the quantile value 0.9, whereas the anomalies in Yahoo Dataset₇ to Yahoo Dataset₉ are close to both quantile values 0.9 and 0.1. Therefore, it is possible to detect anomalies by two extreme quantile values. We can consider these extreme quantile values as higher and lower quantile thresholds and derive a lemma. We provide a proof in the appendix section.

Lemma 1: For an univariate dataset \mathcal{D} , the probability of an anomaly $\mathcal{P}(\mathcal{A}) = \mathcal{P}(\mathcal{E} > \alpha_{high}) + \mathcal{P}(\mathcal{F} < \alpha_{low})$, where $\alpha_{high}, \alpha_{low}$ are the higher and lower level quantile thresholds respectively.

The lemma entails the fact that anomalies are trapped outside the high and low quantile threshold values. The bound is independent of data distribution as quantiles assume nominal distributional characteristics.

3 LSTM with Parameterized Elliot Activation (PEF)

We introduce the novel parameterized Elliot activation function PEF, an adaptive variant of usual activation, wherein we modify the LSTM architecture by replacing the activation function of the LSTM gates with PEF as follows.

A single LSTM block is composed of four major components: an input gate, a forget gate, an output gate, and a cell state. We have applied the parameterized Elliot Function (PEF) as activation.

3.1 Parameterized Elliot Function PEF

PEF is represented by

$$f(x) = \frac{\alpha x}{1 + |x|} \quad (1)$$

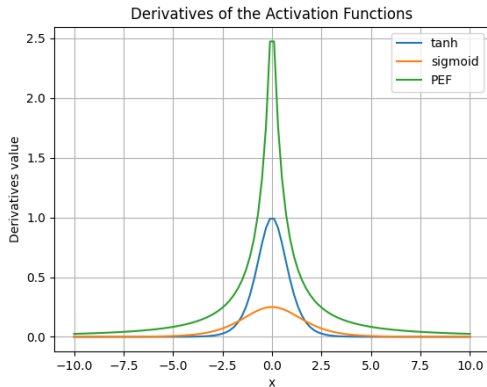
with the first order derivative of PEF as: $f'(x) = \frac{\alpha}{(|x|+1)^2}$. The function is equal to 0, and the derivative is also equal to the parameter α at the origin. After the introduction of the PEF, the hidden state equation is: $h_t = O_t \alpha_c PEF(C_t)$. By chain rule,

$$\frac{\partial J}{\partial \alpha_c} = \frac{\partial J}{\partial \alpha_c} = \frac{\partial J}{\partial h_t} O_t * Elliot(C_t)$$

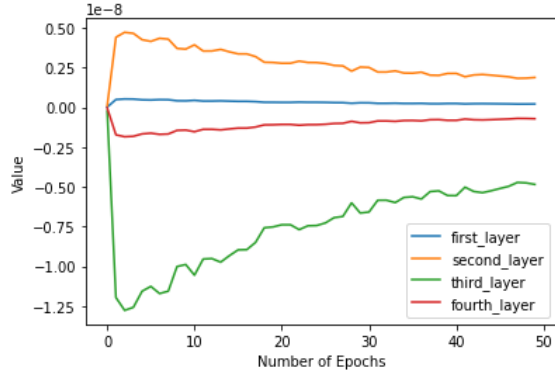
. After each iteration, the α_c is updated by gradient descent $\alpha_c^{(n+1)} = \alpha_c^n + \delta * \frac{\partial J}{\partial \alpha_c}$ (See appendix C for back propagation of LSTM with PEF). Salient features of the PEF are:

1. The α in equation 1 is learned during the back-propagation like other weight parameters of the LSTM model. Hence, this parameter, which controls the shape of the activation, is learned from data. Thus, if the dataset changes, so does the final form of the activation, which saves the “parameter tuning” effort.
2. The cost of saturation of standard activation functions impedes training and prediction, which is an important barrier to overcome. While PEF derivative also saturates as the $|x|$ increases, the saturation rate is less than other activation functions, such as \tanh , sigmoid .
3. PEF further decreases the rate of saturation in comparison to the non-parameterized Elliot function.

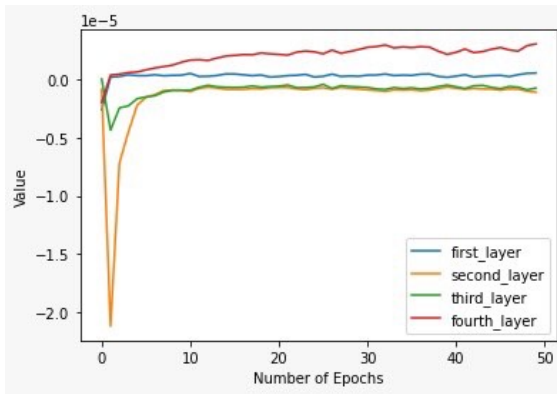
To the best of our knowledge, insights on 'learning' the parameters of an activation function are not available in literature except for the standard smoothness or saturation properties activation functions are supposed to possess. It is, therefore, worthwhile to investigate the possibilities of learning an activation function within a framework or architecture that uses the inherent patterns and variances from data.



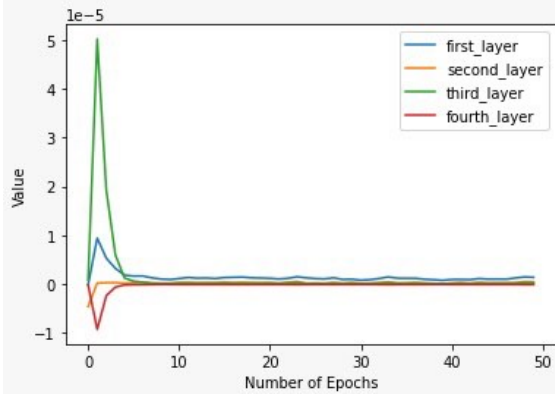
(a) Derivatives comparisons of various activation functions.



(b) LSTM values for 4 layers and 50 epochs using PEF as activation function using AWS2.



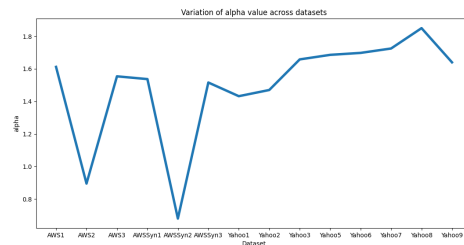
(c) LSTM values for 4 layers and 50 epochs using Sigmoid as activation function using AWS2.



(d) LSTM values for 4 layers and 50 epochs using Tanh as activation function using AWS2.

Dataset	α after training	α initial value
AWS Dataset ₁	1.612	0.1
AWS Dataset ₂	0.895	0.1
AWS Dataset ₃	1.554	0.1
AWS DatasetSyn ₁	1.537	0.1
AWS DatasetSyn ₂	0.680	0.1
AWS DatasetSyn ₃	1.516	0.1
Yahoo Dataset ₁	1.432	0.1
Yahoo Dataset ₂	1.470	0.1
Yahoo Dataset ₃	1.658	0.1
Yahoo Dataset ₅	1.686	0.1
Yahoo Dataset ₆	1.698	0.1
Yahoo Dataset ₇	1.725	0.1
Yahoo Dataset ₈	1.850	0.1
Yahoo Dataset ₉	1.640	0.1

Table 2: Different α values for each Dataset after the training.



(e) The final α values learn on each dataset. We can see the final α value is different for different datasets.

Figure 3: Slow saturation rate as well as behavioral comparison of the different layers of LSTM model after the introduction of PEF with other activation functions. It also shows the final value of the learned parameter α on various datasets.

3.2 PEF saturation

The derivative of the PEF is represented by: $= \frac{\alpha}{x^2} EF^2$. While the derivatives of the sigmoid and tanh are dependent on x , PEF is dependent on both α and x . Even if $\frac{EF^2(x)}{x^2}$ saturates, the learned parameter α will help the PEF escape saturation. The derivatives of the sigmoid, tanh saturate when $x > 5$ or $x < -5$. However, it is not true with PEF as evident from fig 3a. As empirical evidence, the layer values for every epoch of the model are captured using various activation functions like PEF, sigmoid and tanh. It is observed that, after about 10 epochs, the values of the layers becomes more or less constant for sigmoid and tanh (fig 3c and fig 3d), indicating their values have already saturated whereas for PEF, variation can be seen till it reaches 50 epochs (fig 3b). This shows that in comparison to sigmoid and tanh as activation functions, PEF escapes saturation due to its learned parameter α . *The parameter α in PEF changes its value as the model trains over the training dataset while using PEF as the activation function. Since it is a self training parameter, it returns different values for different datasets at the end of training. These values have been documented in table 2 and plotted in fig 3e. Table 2 demonstrates the variations in α values across multiple datasets as these values get updated.*

4 Experiment

In this section, we have evaluated the performance of the quantile-LSTM techniques on multiple datasets. We have identified multiple baseline methods, such as iForest, Elliptic envelope, Autoencoder and several deep learning based approaches for comparison purposes (See section 5 for more details on baseline methods).¹

4.1 Datasets

The dataset properties have been shown in Table 11 of Appendix E. A total of 29 datasets, including real industrial datasets and synthetic datasets, have been considered in the experiments. The industrial datasets include Yahoo web-scope², AWS cloudwatch³, GE. There are a couple of datasets with either one or few anomalies, such as AWS₁, AWS₂. We have injected anomalies in AWS, Yahoo, and GE datasets to produce synthetic data for fair comparison purposes. The datasets are univariate, unimodal or binodal and follow mostly Weibull, Gamma and Log normal distribution. The highest anomaly percentage is 1.47 (GE Dataset₂), whereas AWS Dataset₂ has reported the lowest percentage of anomaly i.e. 0.08 (For more details see Table 11 2 of Appendix E).

4.2 Results-Industrial Datasets

Table 3 demonstrates the performance comparison of various LSTM techniques. Precision and Recall, two performance metrics, are shown in the table. The Median-LSTM has achieved Recall 1 in most datasets (10 out of 15 datasets). In comparison to existing benchmarks, LSTM methods are SOTA on most of the datasets in terms of Recall. For comparison purposes, we have first compared the Recall. If the Recall is the same for two different methods, then we have compared the Precision. The method which has a higher Recall and Precision will be considered as a better performer. In AWS datasets, most of the techniques have achieved the highest Recall apart from DAGMM and DevNet. DevNet needs minimum two anomalies hence it is not applicable for AWS1 and AWS2. However, as per Precision, iqr-LSTM has performed better than other methods. In the case of GE1, DevNet has produced a better result, whereas quantile based LSTM techniques has outperformed others on GE₂. Median-LSTM has demonstrated better result in Ambient temperature. In the case of Yahoo datasets, Median-LSTM has achieved the highest Recall on four datasets; however, quantile-LSTM and iqr-LSTM have produced better results on several datasets. For example, Median-LSTM and iqr-LSTM both achieved Recall 1 on Yahoo₁. However, if we compare the Precision, iqr-LSTM has shown better results. It is evident from the table 3 that all these LSTM versions are performing very well on these industrial datasets. We compared our method with a recent anomaly detection method based on Graph Neural Network (GNN) [2] We observe that GNN has not shown superior performance in comparison to the quantile based technique. For example, GNN's recall value is less in comparison to the recall value of 1 quantile based techniques have produced (on AWS2, AWS3, Yahoo1, Yahoo2, Yahoo9). In terms of precision, GNN produced better results than quantile LSTM only on two datasets, namely, Yahoo1 and Yahoo9.

Table 4 shows the comparison with other baseline algorithms on multiple synthetic datasets. As in the previous table, Recall and Precision have been shown as performance metrics. As per these metrics, quantile-based approaches have outperformed iForest and other deep learning based algorithms on 7 out of 13 datasets. If we consider the Precision

¹LSTM code: <https://github.com/PreyankM/Quantile-LSTM>

²<https://webscope.sandbox.yahoo.com/>

³<https://github.com/numenta/NAB/tree/master/data>

Dataset	Anomaly	iqr-LSTM		Median-LSTM		quantile-LSTM		Autoencoder		GAN		DAGMM		DevNet		iForest		Envelope	
		Precision	Recall	Precision	Recall	Precision	Recall	Precision	Recall	Precision	Recall	Precision	Recall	Precision	Recall	Precision	Recall	Precision	Recall
AWS1	1	0.5	1	0.052	1	0.041	1	0.045	1	0.047	1	0.125	1	NA	NA	0.0087	1	0.009	1
AWS2	2	0.13	1	0.22	1	0.0042	1	0.1	0.5	0.18	1	0.11	1	NA	NA	0.0062	1	0.04	1
AWS3	1	1	1	0.37	1	0.0181	1	0.0344	1	0.055	1	0	0	NA	NA	0.005	1	0.006	1
Ambient temperature	1	0.03	1	0.0769	1	0.02	1	0.055	1	0	0	0	0	NA	NA	0.01	1	0.02	1
GE1	3	0.019	1	0.048	1	0.0357	1	0.093	1	0.041	0.33	0	0	0.12	1	0.004	1	0.2	1
GE2	8	1	1	0.66	1	1	1	1	1	0	0	0.8	1	0.8	1	0.16	1	0.034	1
Yahoo1	2	0.076	1	0.0363	1	0.0465	1	1	0.5	0.066	1	0.07	0.5	0	0	0.005	1	0.009	1
Yahoo2	8	0.75	0.375	0.8	1	1	0.375	1	0.25	0.19	0.625	0.10	0.25	0	0	0.04	0.875	0.055	1
Yahoo3	8	0.615	1	0.114	0.675	0.088	1	0.023	0.25	0.11	0.875	0.15	0.62	0.39	0.5	0.04	0.875	0.032	0.875
Yahoo5	9	0.048	0.33	0.1	0.33	0.022	0.66	0.05	0.33	0	0	0.23	0.33	0.67	1	0.029	0.66	0.029	0.66
Yahoo6	4	0.12	1	0.222	1	0.0275	1	0.048	1	0	0	0.041	1	1	1	0.0073	1	0.0075	1
Yahoo7	11	0.096	0.54	0.16	0.63	0.066	0.54	0.083	0.45	0.035	0.54	0.058	0.09	0.33	0.29	0.0082	0.33	0.017	0.54
Yahoo8	10	0.053	0.7	0.142	0.8	0.028	0.3	0	0	0	0	0	0	0.063	0.11	0.01	0.6	0.010	0.6
Yahoo9	8	1	0.75	0.333	1	0.0208	0.75	1	0.37	0	0	0.5	0.375	0.07	0.8	0.04	1	0.047	1

Table 3: Performance comparison of various quantile LSTM techniques with other state of the art algorithms.

Dataset	Anomaly	iqr-LSTM		Median-LSTM		quantile-LSTM		iForest		Envelope		Autoencoder		GAN		DAGMM		DevNet	
		Precision	Recall	Precision	Recall	Precision	Recall	Precision	Recall	Precision	Recall	Precision	Recall	Precision	Recall	Precision	Recall	Precision	Recall
AWS_syn1	11	0.769	0.909	0.687	1	1	0.909	0.034	1	0.10	1	1	0.63	0.84	1	0.71	0.90	0.09	0.73
AWS_syn2	22	0.7	1	0.733	1	0.6875	1	0.065	1	0.33	1	0.5	0.63	0.70	1	0.56	1	0.44	0.27
AWS_syn3	11	1	0.9	0.47	1	1	1	0.025	1	0.072	1	0.64	0.5	0.68	1	0	0	0.2	0.45
GE_syn1	13	0.0093	1	0.203	1	0.071	0.769	0.0208	1	0.135	1	0.23	0.11	0.25	0.61	0	0	0.33	1
GE_syn2	18	0.0446	1	1	1	1	1	0.3	1	0.409	1	1	0.38	0.9	1	0.9	1	0.9	1
Yahoo_syn1	12	1	1	0.217	0.833	0.375	1	0.027	1	0.056	1	1	0.83	0.31	1	0.29	0.41	0	0
Yahoo_syn2	18	0.181	0.55	0.653	0.944	1	0.611	0.233	1	0.124	1	1	0.42	1	0.61	0.55	0.61	0	0
Yahoo_syn3	18	0.89	0.94	0.3333	0.555	0.6	1	0.0410	1	0.0762	0.944	1	0.88	0.81	0.71	0.3	0.66	0.17	0.63
Yahoo_syn5	19	0.081	0.52	0.521	0.631	0.0625	0.578	0.03125	0.842	0.0784	0.842	0.15	0.47	0.42	0.53	0.52	0.52	0.73	0.92
Yahoo_syn6	14	0.065	0.85	0.65	0.928	0.764	0.928	0.01825	1	0.00761	0.285	0.05	0.28	0.8	0.29	0.041	0.28	0	0
Yahoo_syn7	21	0.61	0.59	0.375	0.714	0.411	0.66	0.032	0.952	0.052	0.85	0.18	0.42	0.14	0.38	0.058	0.047	0.11	0.64
Yahoo_syn8	20	0.32	0.65	0.482	0.823	0.197	0.7	0.0192	0.75	0.023	0.7	0.009	0.05	0.25	0.1	0	0	0.23	0.64
Yahoo_syn9	18	1	0.77	1	1	1	0.94	0.053	1	0.048	1	0.875	0.388	0.72	1	0.57	0.22	0.03	0.29

Table 4: Performance comparison of various quantile LSTM techniques on synthetic datasets with other state of the art algorithms.

alone, the quantile LSTM based techniques have demonstrated better performance on 10 synthetic datasets. There are multiple reasons for the better performance demonstrated by the quantile based LSTM approaches. First is the efficacy of the LSTM, which is well documented. Median-LSTM has detected the anomalies for each time period utilizing mean and standard deviation. It also has helped to capture the trend and seasonality. quantile-LSTM do not have any predefined threshold, which has improved their performance. Additionally, the flexibility of the parameter α in determining the shape of the activation helped in isolating the anomalies. This is evident from Fig 3e which represents the variation in α values of the PEF function across the datasets. α has been initialized to 1.5 for all the datasets.

4.3 Results-Non-Industrial Datasets

We have tested our approach on non-industrial datasets shown in Table 5. Here, Deviation Networks gives NA because it does not work for single anomaly containing datasets. On analysis of the results, we find that the quantile based technique is better in three of the seven datasets while Autoencoder is better for two of the seven datasets.

Dataset	Anomaly	quantile-LSTM		Autoencoder		GAN		DevNet		iForest		Envelope	
		Precision	Recall	Precision	Recall	Precision	Recall	Precision	Recall	Precision	Recall	Precision	Recall
TravelTime ₃₈₇	3	0.011	0.67	1	0.33	0.024	0.33	0.01	0.33	0.0039	0.6667	0.0107	0.6667
TravelTime ₄₅₁	1	0.006	1	0	0	0.016	1	NA	NA	0.0028	1	0.0062	1
Occupancy ₆₀₀₅	1	0.03	1	0	0	0.007	1	NA	NA	0.0019	1	0.0042	1
Occupancy _{t4013}	2	0.06	1	0.438	0.5	0.014	0.5	0.02	1	0.0038	1	0.0078	1
Speed ₆₀₀₅	1	0.014	1	0.103	1	0.009	1	NA	NA	0.002	1	0.0038	1
Speed ₇₅₇₈	4	0.086	1	0.792	1	0.2	0.9	0.16	0.75	0.0153	1	0.0247	1
Speed _{t4013}	2	0.053	1	0.75	0.5	0.043	1	0.1	1	0.0036	1	0.007	1

Table 5: Performance comparison of quantile LSTM techniques on various non-industrial datasets

4.4 Comparison between Elliot Function and PEF

In order to compare the performance of the Elliot function and parameterized Elliot function (PEF) as activation functions, we experimented with them by using them as activation functions in the LSTM layer of the models and comparing the results after they run on multiple datasets. The results are shown in Table 6. According to the data gathered after running the models, we found that parameterized Elliot function has better Precision and Recall for as except for four of the datasets. Thus, we could conclude that using parameterized Elliot function as an activation function gave better performance for quantile-LSTM.

Dataset	Elliot Function		Parameterized Elliot Function	
	Precision	Recall	Precision	Recall
AWS Dataset ₁	0	0	0.041	1
AWS Dataset ₂	0.002	1	0.0042	1
AWS Dataset ₃	0.04	1	0.0181	1
AWS DatasetSyn ₁	0.02	0.73	1	0.909
AWS DatasetSyn ₂	0.39	0.77	0.6875	1
AWS DatasetSyn ₃	0.06	0.73	1	1
Yahoo Dataset ₁	0.006	0.25	0.0465	1
Yahoo Dataset ₂	0.02	1	1	0.375
Yahoo Dataset ₃	0.05	1	0.088	1
Yahoo Dataset ₅	0.001	0.33	0.022	0.66
Yahoo Dataset ₆	0.002	0.17	0.0275	1
Yahoo Dataset ₇	0.03	0.09	0.066	0.54
Yahoo Dataset ₈	0.017	0.4	0.028	0.3
Yahoo Dataset ₉	0.43	0.75	0.0208	0.75
Yahoo DatasetSyn ₁	0.14	0.86	0.375	1
Yahoo DatasetSyn ₂	0.04	0.72	1	0.611
Yahoo DatasetSyn ₃	0.1	0.78	0.6	1
Yahoo DatasetSyn ₅	0.004	0.31	0.0625	0.578
Yahoo DatasetSyn ₆	0.015	0.69	0.764	0.928
Yahoo DatasetSyn ₇	0.35	0.43	0.411	0.66
Yahoo DatasetSyn ₈	0.024	0.5	0.197	0.7
Yahoo DatasetSyn ₉	0.27	0.67	1	0.94

Table 6: Comparison of Precision and Recall score for LSTM with Elliot Function and PEF as Activation Function

4.5 Impact of Varying Thresholds

Deep-learning based algorithms such as Autoencoder [17], GAN [25], DAGMM [28] and DevNet [14] consider upper threshold and lower thresholds on reconstruction errors or predicted value. To understand the impact of different thresholds on the performance, we have considered three baseline algorithms GAN, Autoencoder and Devnet. The baseline methods have considered three different sets of threshold values for upper and lower thresholds. The sets are shown in column head of tables 7, 8 and 9, where the first threshold is the upper percentile and the second threshold is the lower percentile. In contrast, q-LSTM is robust against thresholds as data sets vary i.e. it captures all anomalies successfully within the 0.1 and 0.9 quantile threshold.

GAN	99.25 and 0.75		99.75 and 0.25		99.9 and 0.1	
Dataset	Precision	Recall	Precision	Recall	Precision	Recall
Yahoo Dataset ₁	0.09	1	0.25	1	0.5	1
Yahoo Dataset ₂	0.348	1	0.333	0.375	0.4	0.25
Yahoo Dataset ₃	0.28	0.5	0.444	0.286	0.28	0.5
Yahoo Dataset ₅	0	0	0.375	0.333	0.6	0.333
Yahoo Dataset ₆	0.5	0.5	0.5	1	0.182	1
Yahoo Dataset ₇	0.154	0.364	0.3	0.273	0.5	0.182
Yahoo Dataset ₈	0.038	0.1	0.1	0.1	0.25	0.1
Yahoo Dataset ₉	0.192	0.625	0.5	0.625	0.5	0.25

Table 7: Comparison of Precision and Recall score for GAN with varying thresholds for anomaly Upper Bound and Lower Bound

Autoencoders	99.25 and 0.75		99.75 and 0.25		99.9 and 0.1	
Dataset	Precision	Recall	Precision	Recall	Precision	Recall
Yahoo Dataset ₁	0.5	0.07	0.5	0.036	0.5	0.019
Yahoo Dataset ₂	0.5	0.4	0.333	0.5	0.2	0.5
Yahoo Dataset ₃	0.44	0.5	0.4	0.5	0.25	0.333
Yahoo Dataset ₅	0.5	0.5	0.5	0.5	0.5	0.5
Yahoo Dataset ₆	0.5	1	1	1	0.25	1
Yahoo Dataset ₇	0.5	0.5	0.5	0.5	0.5	0.5
Yahoo Dataset ₈	0.875	0.875	0.375	0.375	0.5	0.75
Yahoo Dataset ₉	0.75	0.5	0.25	0.5	0.5	0.5

Table 8: Comparison of Precision and Recall score for Autoencoders with varying thresholds for anomaly Upper Bound and Lower Bound

Devnet	99.25 and 0.75		99.75 and 0.25		99.9 and 0.1	
Dataset	Precision	Recall	Precision	Recall	Precision	Recall
Yahoo Dataset ₁	0.002	1	0.002	1	0.001	1
Yahoo Dataset ₂	0.005	1	0.005	1	0.005	1
Yahoo Dataset ₃	0.0078	1	0.0078	1	0.0078	1
Yahoo Dataset ₅	0.111	0.5	0.333	0.5	0.333	0.5
Yahoo Dataset ₆	0.167	1	0.5	1	0.5	0.667
Yahoo Dataset ₇	0.054	0.2	0.125	0.2	0.25	0.2
Yahoo Dataset ₈	0	0	0	0	0	0
Yahoo Dataset ₉	0	0	0	0	0	0

Table 9: Comparison of Precision and Recall score for Devnet with varying thresholds for anomaly Upper Bound and Lower Bound

It is evident from the above tables that performance varies significantly based on the thresholds decided by the algorithm. Therefore it is very important to decide on a correct threshold that can identify all the probable anomalies from the dataset.

4.6 Experiments on Normal Instances

A relevant question to ask is: how would the anomaly detection methods perform on normal data instances that does not have any anomaly? We investigate this by removing anomalies from some data sets. We observe that on these data sets (AWS1, AWS2, AWS3, Yahoo1, Yahoo2, Yahoo3), q-LSTM and its variants reported very negligible false alarms (Average 40 false alarms) while other state-of-the-art methods, such as iForest, Elliptic Envelope produce higher flag false positives. Elliptic envelope has reported, on average, 137 false alarms whereas iForest reported an average of 209 false alarms across the datasets. Autoencoder and GAN, both have reported average false alarms 46 and 123 respectively, which is higher than the false positive rate of q-LSTM. This establishes the robustness of the proposed method.

5 Related Work

Well-known supervised machine learning approaches such as Linear Support Vector Machines (SVM), Random Forest (RF), and Random Survival Forest (RSF) [23, 22] have been explored for fault diagnosis and the lifetime prediction of industrial systems. [1] have explored SVM and RF to detect intrusion based on the anomaly in industrial data. Popular unsupervised approaches, such as Anomaly Detection Forest [20], and K-means based Isolation Forest [7] try to isolate the anomalies from the normal dataset. These methods do not require labeled data. [7] considered K-means based anomaly isolation, but the approach is tightly coupled with a clustering algorithm. Anomaly Detection Forest like k-means based iForest requires a training phase with a subsample of the dataset under consideration. A wrong selection of the training subsample can cause too many false alarms. The notion of “likely invariants” uses operational data to identify a set of invariants to characterize the normal behavior of a system, which is similar to our strategy. Such as an approach has been attempted to discover anomalies of cloud-based systems [16]. However, such

an approach requires labeling of data and retuning of parameters when the nature of datasets vary. Recently, Deep Learning (DL) models based on auto-encoders, long-short term memory [4, 26] are increasingly gaining attention for anomaly detection. [24] have proposed an integrated model of Convolutional Neural Network (CNN) and LSTM based auto-encoder for Yahoo Webscope time-series anomaly detection. For reasons unknown, [24] have taken only one Yahoo Webscope data to demonstrate their approach’s efficacy. The DeepAnT [12] approach employs DL methods and it uses unlabeled data for training. However, the approach is meant for time-series data sets such as Yahoo Webscope, Real traffic, AWS cloudwatch. A stacked LSTM [10] is used for time series anomaly prediction, and the network is trained on a normal dataset. The hierarchical Temporal Memory (HTM) method has been applied recently on sequential streamed data and compared with other time series forecasting models [13]. The authors in [18] have performed online time-series anomaly detection using deep RNN. The incremental retraining of the neural network allows to the adoption of concept drift across multiple datasets. There are various works [11, 19], which attempt to address the data imbalance issue of the anomaly datasets since anomalies are very rare and occur occasionally. Hence they propose semi-supervised approaches. However, the semi-supervised approach cannot avoid the expensive dataset labeling. Some approaches [27] apply predefined thresholds, such as fixed percentile values to detect the anomalies. However, a fixed threshold value may not be equally effective on different domain datasets. Deep Autoencoding Gaussian Mixture Model (DAGMM) is an unsupervised DL-based anomaly detection algorithm [27], where it utilizes a deep autoencoder to generate a low-dimensional representation and reconstruction error for each input data point and is further fed into a Gaussian Mixture Model (GMM). Deviation Network(DevNet) [14] is a novel method that harnesses anomaly scoring networks, Z-score based deviation loss, and Gaussian prior together to increase efficiency for anomaly detection.

6 Discussion and Conclusion

In this paper, we have proposed multiple versions of the SoTA anomaly detection algorithms along with a forecasting-based LSTM method. We have demonstrated that combining the quantile technique with LSTM can be successfully implemented to detect anomalies in industrial and non-industrial datasets without label availability for training. We have also exploited the parameterized Elliot activation function and shown anomaly distribution against quantile values, which helps in deciding the quantile anomaly threshold. The design of a flexible form activation, i.e., PEF, also helps in accommodating variance in the unseen data as the shape of the activation is learned from data. PEF, as seen in Table 6 captures anomalies better than vanilla Elliot. The quantile thresholds are generic and will not differ for different datasets. The proposed techniques have addressed the data imbalance issue and expensive training dataset labeling in anomaly detection. These methods are useful where data is abundant. Traditional deep learning-based methods use classical conditional means and assume random normal distributions as the underlying structure of data. These assumptions make the methods vulnerable to capturing the uncertainty in prediction and make them incapable of modeling tail behaviors. Quantile in LSTM (for time series data) is a robust alternative that we leveraged in isolating anomalies successfully. This is fortified by the characteristics of quantiles making very few distributional assumptions. The distribution-agnostic behavior of Quantiles turned out to be a useful tool in modeling tail behavior and detecting anomalies. Anomalous instances, by definition, are rare and could be as rare as just one anomaly in the entire data set. Our method detects such instances (singleton anomaly) while some, recent state of art algorithms such as DAGMM require at least two anomalies to be effective. Extensive experiments on multiple industrial timeseries datasets (Yahoo, AWS, GE, machine sensors, Numenta and VLDB Benchmark data) and non-time series data show evidence of effectiveness and superior performance of LSTM-based quantile techniques in identifying anomalies. The proposed methods have a few drawbacks 1. quantile based LSTM techniques are applicable only on univariate datasets. 2. A few of the methods such as quantile-LSTM, iqr-LSTM have a dependency on multiple thresholds. We intend to introduce the notion of multiple dimensions in our quantile-based approaches to detect anomalies in multivariate time series data in the future.

References

- [1] D. D. S. Anton, S. Sinha, and H. Dieter Schotten. Anomaly-based intrusion detection in industrial data with svm and random forests. In *2019 International Conference on Software, Telecommunications and Computer Networks (SoftCOM)*, 2019. doi: [10.23919/softcom.2019.8903672](https://doi.org/10.23919/softcom.2019.8903672).
- [2] A. Deng and B. Hooi. Graph neural network-based anomaly detection in multivariate time series. In *Proceedings of the AAAI Conference on Artificial Intelligence*, volume 35, pages 4027–4035, 2021.
- [3] Ted Dunning. The t-digest: Efficient estimates of distributions. *Software Impacts*, 7, 2021.
- [4] S.M. Erfani, S. Rajasegarar, S. Karunasekera, and C. Leckie. High-dimensional and large-scale anomaly detection using a linear one-class svm with deep learning. *Pattern Recognit*, 58:121–134, 2016.

- [5] J. L. Horowitz. A smoothed maximum score estimator for the binary response model. *Econometrica*, 60(3):505–531, 1992.
- [6] A. Jinwon and S. Ch. Variational autoencoder based anomaly detection using reconstruction probability. In *Special Lecture on IE*, pages 1–18, 2015.
- [7] P. Karczmarek, A. Kiersztyn, W. Pedrycz, and E. Al. K-means-based isolation forest. *Knowledge-Based Systems*, 195, 2020.
- [8] Roger Koenker. *Quantile Regression*. Cambridge University Press, 2005.
- [9] T. F. Liu, M. K. Ting, and Z. H. Zhou. Isolation forest. In *2008 Eighth IEEE International Conference on Data Mining*, page 273–280, December 2008. doi: [10.1109/ICDMW.2016.0046](https://doi.org/10.1109/ICDMW.2016.0046).
- [10] P. Malhotra, L. Vig, G.G. Shroff, and P. Agarwal. Long short term memory networks for anomaly detection in time series. In *European Symposium on Artificial Neural Networks, Computational Intelligence and Machine Learning*, pages 89–94, 2015.
- [11] A. Morales-Forero and S. Bassetto. Case study: A semi-supervised methodology for anomaly detection and diagnosis. In *In 2019 IEEE International Conference on Industrial Engineering and Engineering Management (IEEM)*, pages 1031–1037, 2019.
- [12] M. Munir, A. S. Siddiqui, A. Dengel, and S. Ahmed. Deepant: A deep learning approach for unsupervised anomaly detection in time series. *IEEE Access*, 1(1):1085–1100, 2018. doi: [10.1109/access.2018.2886457](https://doi.org/10.1109/access.2018.2886457).
- [13] E. N. Osegi. Using the hierarchical temporal memory spatial pooler for short-term forecasting of electrical load time series. *Applied Computing and Informatics*, 7(2):264–278, 2021.
- [14] Guansong Pang, Chunhua Shen, and Anton van den Hengel. Deep anomaly detection with deviation networks. In *Proceedings of the 25th ACM SIGKDD international conference on knowledge discovery & data mining*, pages 353–362, 2019.
- [15] P. J. Rousseeuw and K. V. Driessen. A fast algorithm for the minimum covariance determinant estimator. *Technometrics*, 41(3):212–223, 1999. doi: [10.1080/00401706.1999.10485670](https://doi.org/10.1080/00401706.1999.10485670).
- [16] A. Russo, S. Pecchia, and S. Sarkar. Assessing invariant mining techniques for cloud-based utility computing systems. *IEEE Transactions on Services Computing*, 13(1):44–58, 2020.
- [17] M. Sakurada and T. Yairi. Anomaly detection using autoencoders with nonlinear dimensionality reduction. In *Proceedings of the MLSDA 2014 2nd Workshop on Machine Learning for Sensory Data Analysis - MLSDA'14*, pages 1031–1037, 2014.
- [18] S. Saurav, P. Malhotra, V. T. N. Gugulothu, L. Vig, P. Agarwal, and G. Shroff. Online anomaly detection with concept drift adaptation using recurrent neural networks. In *Proceedings of the ACM India Joint International Conference on Data Science and Management of Data, ser. CoDS-COMAD*, page 78–87, 2018.
- [19] P. Sperl, J. P. Schulze, and K. B. ottinger. A3: Activation anomaly analysis. *CoRR*, 2020.
- [20] J. Sternby, E. Thormarker, and M. Liljenstam. Anomaly detection forest. In *ECAI*, 2020.
- [21] A. Tambwekar, A. Maiya, S. Dhavala, and S. Saha. Estimation and applications of quantiles in deep binary classification. *IEEE Transactions on Artificial Intelligence*, 3(2):275–286, 2022.
- [22] K. N. Verma, R. K. Sevakula, and R. Thirukovalluru. Pattern analysis framework with graphical indices for condition-based monitoring. *IEEE Transactions on Reliability*, 66(4):1085–1100, 2017. doi: [10.1109/TR.2017.2729465](https://doi.org/10.1109/TR.2017.2729465).
- [23] S. Voronov, E. Frisk, and M. Krysander. Data-driven battery lifetime prediction and confidence estimation for heavy-duty trucks. *IEEE Transactions on Reliability*, 67(2):623–639, 2018. doi: [10.1109/TR.2018.2803798](https://doi.org/10.1109/TR.2018.2803798).
- [24] C. Yin, J. Wang S. Zhang, and N. N. Xiong. Anomaly detection based on convolutional recurrent autoencoder for iot time series. *IEEE Transactions on Systems, Man, and Cybernetics: Systems*, pages 1–11, 2020. doi: [10.1109/tsmc.2020.2968516](https://doi.org/10.1109/tsmc.2020.2968516).
- [25] H. Zenati, M. Romain, C. Foo, B. Lecouat, and V. Chandrasekhar. Adversarially learned anomaly detection. In *IEEE International Conference on Data Mining (ICDM)*, pages 727–736, 2018.
- [26] C. Zhou and R. C. Paffenroth. Anomaly detection with robust deep autoencoders. In *Proceedings of the 23rd ACM SIGKDD International Conference on Knowledge Discovery and Data Mining - KDD*, 2017. doi: [10.1145/3097983.3098052](https://doi.org/10.1145/3097983.3098052).
- [27] Bo Zong, Qi Song, Martin Renqiang Min, Wei Cheng, Cristian Lumezanu, Daeki Cho, and Haifeng Chen. Deep autoencoding gaussian mixture model for unsupervised anomaly detection. In *International Conference on Learning Representations*, 2018.

- [28] Bo Zong, Qi Song, Martin Renqiang Min, Wei Cheng, Cristian Lumezanu, Daeki Cho, and Haifeng Chen. Deep autoencoding gaussian mixture model for unsupervised anomaly detection. In *International Conference on Learning Representations*, 2018.

Appendix A Probability Bound

Table 10 shows the probabilities of the anomalies at various quantile thresholds. The table has demonstrated all the 32 datasets considered as part of the experiment section.

Dataset	$\mathcal{P}(\mathcal{E} > 0.95)$	$\mathcal{P}(\mathcal{E} > 0.9)$	$\mathcal{P}(\mathcal{E} > 0.75)$	$\mathcal{P}(\mathcal{F} < 0.25)$	$\mathcal{P}(\mathcal{F} < 0.10)$
AWS Dataset ₁	0	0.01	0.004	0	0
AWS Dataset ₂	0	0.1	0.1	0	0
AWS Dataset ₃	0	0.007	0.0032	0	0
Yahoo Dataset ₁	0	0.014	0.005	0	0
Yahoo Dataset ₂	0	0.105	0.062	0	0
Yahoo Dataset ₃	0	0.103	0.076	0	0
Yahoo Dataset ₄	0	0.014	0.0055	0	0
Yahoo Dataset ₅	0	0.043	0.016	0	0
Yahoo Dataset ₆	0	0.028	0.011	0	0
Yahoo Dataset ₇	0	0.047	0.018	0.0069	0.017
Yahoo Dataset ₈	0	0.011	0.004	0.016	0.041
Yahoo Dataset ₉	0	0.017	0.0069	0.011	0.029
Sensor Dataset ₁	0	0.0344	0.0135	0	0
Sensor Dataset ₂	0	0	0	0.013	0.033
GE Dataset ₁	0	0.003	0.002	0	0
GE Dataset ₂	0	0.05	0.042	0	0
AWS Datasetsyn ₁	0	0.08	0.035	0	0
AWS Datasetsyn ₂	0	0.08	0.035	0	0
AWS Datasetsyn ₃	0	0.1	0.1	0	0
Yahoo Datasetsyn ₁	0	0.074	0.034	0	0
Yahoo Datasetsyn ₂	0	0.21	0.15	0	0
Yahoo Datasetsyn ₃	0	0.13	0.11	0	0
Yahoo Datasetsyn ₅	0	0.08	0.036	0	0
Yahoo Datasetsyn ₆	0	0	0	0.025	0.062
Yahoo Datasetsyn ₇	0	0.047	0.018	0.03	0.076
Yahoo Datasetsyn ₈	0	0.034	0.015	0.026	0.051
Yahoo Datasetsyn ₉	0	0.017	0.0069	0.034	0.088
Sensor Datasetsyn ₁	0	0	0	0.108	0.39
Sensor Datasetsyn ₂	0	0	0	0.146	0.36
GE DatasetSyn ₁	0	0.017	0.0104	0	0
GE DatasetSyn ₂	0	0.11	0.096	0	0

Table 10: Various probability values on different quantile threshold parameters.

Appendix B Lemma

Lemma 1:

For an univariate dataset \mathcal{D} , the probability of an anomaly $\mathcal{P}(\mathcal{A}) = \mathcal{P}(\mathcal{E} > \alpha_{high}) + \mathcal{P}(\mathcal{F} < \alpha_{low})$, where $\alpha_{high}, \alpha_{low}$ are the higher and lower level quantile thresholds respectively.

Proof. A datapoint is declared an anomaly if its quantile value is higher than α_{high} or lower than α_{low} . Here $\alpha_{high}, \alpha_{low}$ are the higher and lower quantile threshold value. $\mathcal{P}(\mathcal{E} > \alpha_{high})$ is the probability of an anomaly whose quantile value is higher than α_{high} . On the other side, $\mathcal{P}(\mathcal{F} < \alpha_{low})$ is the probability of quantile value of anomalous datapoint lower than α_{low} . Hence the presence of an anomaly in a dataset is possible if one of the events is true. Therefore

$$\begin{aligned} \mathcal{P}(\mathcal{A}) &= P(\mathcal{E} > \alpha_{high} \cup \mathcal{F} < \alpha_{low}) \\ \mathcal{P}(\mathcal{A}) &= P(\mathcal{E} > \alpha_{high}) + P(\mathcal{F} < \alpha_{low}) - P(\mathcal{E} > \alpha_{high} \cap \mathcal{F} < \alpha_{low}) \end{aligned}$$

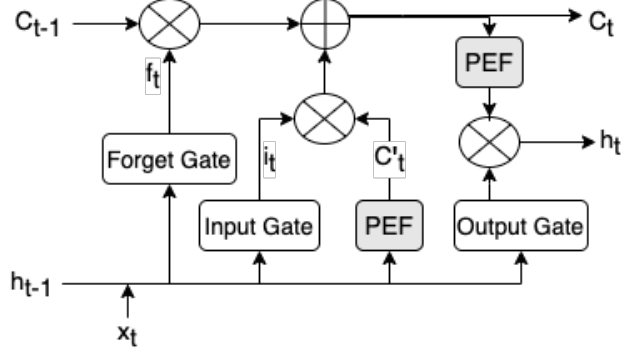


Figure 4: LSTM cell structure

Both the events \mathcal{E}, \mathcal{F} are mutually exclusive. Hence the above Equation can be written as

$$\mathcal{P}(\mathcal{A}) = \mathcal{P}(\mathcal{E} > \alpha_{high}) + \mathcal{P}(\mathcal{F} < \alpha_{low}) \quad (2)$$

□

Appendix C Backpropagation of LSTM with PEF

For backward propagation, it is required to compute the derivatives for all major components of the LSTM. J is the cost function and the relationship between v_t and hidden state h_t is $v_t = w_v * h_t + b_v$. The predicted value $y' = softmax(v_t)$. The derivative of the hidden state can be shown as follow

$$\begin{aligned} \frac{\partial J}{\partial h_t} &= \frac{\partial J}{\partial v_t} \frac{\partial v_t}{\partial h_t} \\ \frac{\partial J}{\partial h_t} &= \frac{\partial J}{\partial v_t} \frac{\partial (w_v * h_t + b_v)}{\partial h_t} \\ \frac{\partial J}{\partial h_t} &= \frac{\partial J}{\partial v_t} w_v \end{aligned}$$

The variable involved in the output gate is o_t .

$$\begin{aligned} \frac{\partial J}{\partial o_t} &= \frac{\partial J}{\partial h_t} \frac{\partial h_t}{\partial o_t} \\ \frac{\partial J}{\partial o_t} &= \frac{\partial J}{\partial h_t} \frac{\partial (o_t * PEF(C_t))}{\partial o_t} \\ \frac{\partial J}{\partial o_t} &= \frac{\partial J}{\partial h_t} PEF(C_t) \end{aligned}$$

C_t is the cell state and the chain rule for cell state can be written as

$$\frac{\partial J}{\partial C_t} = \frac{\partial J}{\partial h_t} \frac{\partial h_t}{\partial C_t} \quad (3)$$

$\frac{\partial J}{\partial h_t}$ value already we have calculated as part of hidden state equation.

$$\begin{aligned} \frac{\partial h_t}{\partial C_t} &= \frac{\partial (o_t * PEF(C_t))}{\partial C_t} \\ &= \frac{\alpha o_t}{(|C_t| + 1)^2} \end{aligned}$$

After setting the value of $\frac{\partial h_t}{\partial C_t}$ in equation 4

$$\frac{\partial J}{\partial C_t} = \frac{\partial J}{\partial h_t} \frac{\alpha o_t}{(|C_t| + 1)^2} \quad (4)$$

The chain rule for \hat{c}_t is

$$\frac{\partial J}{\partial \hat{c}_t} = \frac{\partial J}{\partial C_t} \frac{\partial C_t}{\partial \hat{c}_t}$$

We need to derive only $\frac{\partial C_t}{\partial \hat{c}_t}$ since $\frac{\partial J}{\partial C_t}$ is available from equation 5.

$$\begin{aligned} \frac{\partial C_t}{\partial \hat{c}_t} &= \frac{\partial (f_t * C_{t-1} + \hat{c}_t * i_t)}{\partial \hat{c}_t} \\ &= i_t \end{aligned}$$

After replacing the value of $\frac{\partial C_t}{\partial \hat{c}_t}$

$$\frac{\partial J}{\partial \hat{c}_t} = \frac{\partial J}{\partial C_t} * i_t$$

Similar way $\frac{\partial J}{\partial a_c} = \frac{\partial J}{\partial \hat{c}_t} * \frac{\alpha}{(|a_c|+1)^2}$ The following derivatives for input gate

$$\begin{aligned} \frac{\partial J}{\partial i_t} &= \frac{\partial J}{\partial C_t} \hat{c}_t \\ \frac{\partial J}{\partial a_i} &= \frac{\partial J}{\partial C_t} \hat{c}_t (i_t (1 - i_t)) \end{aligned}$$

For forget gate, below are the derivatives

$$\begin{aligned} \frac{\partial J}{\partial f_t} &= \frac{\partial J}{\partial C_t} C_{t-1} \\ \frac{\partial J}{\partial a_f} &= \frac{\partial J}{\partial C_t} C_{t-1} (f_t (1 - f_t)) \end{aligned}$$

Z_t is the concatenation of the h_{t-1}, x_t . The derivatives of the weights are as follow

$$\begin{aligned} \frac{\partial J}{\partial w_f} &= \frac{\partial J}{\partial a_f} Z_t \\ \frac{\partial J}{\partial w_i} &= \frac{\partial J}{\partial a_i} Z_t \\ \frac{\partial J}{\partial w_v} &= \frac{\partial J}{\partial v_t} h_t \\ \frac{\partial J}{\partial w_o} &= \frac{\partial J}{\partial a_o} Z_t \end{aligned}$$

C.1 Parameterized Elliot Function

One of the major benefit of the parameterized Elliot function is that it further decreases the rate of saturation in comparison to the non-parameterize Elliot function. We have applied one parameter α , which controls the shape of the Elliot function. There will be different derivatives if we apply parameterize Elliot function in LSTM.

$$PEF = \frac{\alpha x}{1 + |x|}$$

After the introduction of the PEF, the hidden state equation is as follow

$$h_t = O_t \alpha_c PEF(C_t)$$

As per the chain rule, the derivative for α_c will be

$$\begin{aligned} \frac{\partial J}{\partial \alpha_c} &= \frac{\partial J}{\partial h_t} \frac{\partial O_t \alpha_c Elliot(C_t)}{\partial \alpha_c} \\ \frac{\partial J}{\partial \alpha_c} &= \frac{\partial J}{\partial h_t} O_t * Elliot(C_t) \end{aligned}$$

After each iteration, the α_c is updated as per equation 5.

$$\alpha_c^{(n+1)} = \alpha_c^n + \delta * \frac{\partial J}{\partial \alpha_c} \quad (5)$$

Similarly, we can derive $\alpha_c \hat{c}_t$ and update the parameter.

Appendix D Intuition with An Example:

It is hypothesized that, in neural networks, the logistic layer output $\text{softmax}(b+Wh)$ might initially rely more on the biases b and hence push the activation value h towards 0, thus resulting in error gradients of smaller values. They referred to this as the saturation property of neural networks. This results in slower training and prevents the gradients from propagating backward until the layers close to the input learn. This saturation property is observed in the sigmoid. The sigmoid is non-symmetric around zero and obtains smaller error gradients when the sigmoid outputs a value close to 0. Similarly, tanh in all layers tends to saturate towards 1, which leads to layer saturation. All the layers attain a particular value, which is detrimental to the propagation of gradients. However, this issue of attaining saturation would be less pronounced in cases where two different activation functions are used. Since each activation function behaves differently in terms of gradients, i.e., sigmoid outputs are in the range $[0,1]$, and the gradients are minimum at the maximum and minimum values of the function. The tanh on the other hand, has minimum gradients at -1 and 1 and reaches its maximum at 0. Therefore, even if the layers begin to saturate to a common value, some of the layers would escape the saturation regime of their activations and would still be able to learn essential features. As an outcome, this might result in fewer instances of vanishing gradients. This assumption would mean that networks with two different activations would learn faster and converge faster to a minima, and the same premise is supported by a Convergence study (details in section V). As demonstrated by Glorot and Bengio, if the saturation ratio of layers is less pronounced, it leads to better results in terms of accuracy. A standard neural network with N layers is given by $h^l = \sigma(h^{l-1}W^l + b)$ and $s^l = h^{l-1}W^l + b$. Here h^l is the output of the first hidden layer, σ is a non-linear activation function, and b is the bias. We compute the gradients as $\frac{\partial Cost}{\partial s_k^l} = f'(s_k^l)W_{k,\cdot}^l \frac{\partial Cost}{\partial s^{l+1}}$, $\frac{\partial Cost}{\partial W_{m,n}^l} = z_l^i \frac{\partial Cost}{\partial s_k^l}$. Now, we find the variances of these values. As the network propagates, we must ensure that the variances are equal to keep the information flowing. Essentially, when $\forall(l, l'), Var[h^l] = Var[h^{l'}]$, it ensures that forward propagation does not saturate, and when $\forall(l, l'), Var[\frac{\partial Cost}{\partial s^l}] = Var[\frac{\partial Cost}{\partial s^{l'}}]$, it ensures that backward propagation flows at a constant rate. Now, what remains is to calculate these variance values. Let us consider an elaborate example.

Firstly, we attempt to find variance for two sigmoid activations in a network. The derivative of each activation output is approximately $0.25(\sigma'(0) = 0.25)$, as the weights are uniformly initialized, and the input features are assumed to have the same variance. Hence,

$$f'(s_k^l) = 0.25$$

$$Var[z^2] = Var[x]((0.25)^2 n_1 Var[W^{1'}] * (0.25)^2 n_2 Var[W^{2'}])$$

We see that this diminishing factor of 0.25^N steeply drops the variance during the forward pass. Similarly, we observe that the gradient,

$$\frac{\partial Cost}{\partial s_k^l} = f'(s_k^l)W_{k,\cdot}^l \frac{\partial Cost}{\partial s^{l+1}}$$

has $f'(s_k^l)$ as one of the factors, and thus the diminishing factor is tied to the variance. Even when $N = 2$ the variance reduces by a factor of $4^4 = 256$.

Let's compute variance for neural network with two hidden layers using sigmoid and tanh activations. For tanh, if the initial values are uniformly distributed around 0, the derivative is $f'(s_k^l) = 1$. Therefore, the variance for the second layer output is, $Var[z^2] = Var[x] * ((0.25)^2 * n_1 * Var[W^{1'}] * n_2 * Var[W^{2'}])$. We see that the diminishing factor is just $4^2 = 16$, and this results in a much better variance when compared to the previous case. Therefore, using different AFs instead of the same implies a reduction in vanishing gradients and results in a much better flow of information because the variance value is preserved for longer.

Appendix E Dataset Properties

Dataset Name	Anomaly%	Size	Missing Data	Modal	Distribution	#Variables	TW/ Period
Publicly available actual industrial data							
AWS Dataset ₁	0.09	1049	No	Unimodal	Weibull	Univariate	84/168
AWS Dataset ₂	0.08	2486	No	Unimodal	Weibull	Univariate	38/152
AWS Dataset ₃	0.066	1499	No	Multimodal	Weibull	Univariate	38/152
Yahoo Dataset ₁	0.14	1421	No	Unimodal	Weibull	Univariate	20/60
Yahoo Dataset ₂	0.54	1462	No	Unimodal	Gamma	Univariate	30/90
Yahoo Dataset ₃	0.55	1440	No	Unimodal	Weibull	Univariate	10/120
Yahoo Dataset ₄	0.28	1422	No	Bimodal	Weibull	Univariate	105/210
Yahoo Dataset ₅	0.63	1421	No	Bimodal	Log-normal	Univariate	24/72
Yahoo Dataset ₆	0.28	1421	No	Multimodal	Weibull	Univariate	74/148
Yahoo Dataset ₇	0.53	1680	No	Unimodal	Weibull	Univariate	125/250
Yahoo Dataset ₈	0.59	1680	No	Unimodal	Log-normal	Univariate	116/232
Yahoo Dataset ₉	0.47	1680	No	Unimodal	Weibull	Univariate	30/90
Machine Temperature Dataset	0.19	501	No	Multimodal	Weibull	Univariate	38/114
Private actual industrial data							
GE Dataset ₁	0.18	1609	No	Unimodal	Exponential	Univariate	117/234
GE Dataset ₂	1.47	544	No	Multimodal	Weibull	Univariate	50/150
Publicly available synthetic industrial data							
AWS DatasetSyn ₁	1.03	1059	No	Unimodal	Exponential	Univariate	84/168
AWS DatasetSyn ₂	0.877	2506	No	Unimodal	Weibull	Univariate	38/152
AWS DatasetSyn ₃	0.72	1509	No	Unimodal	Gamma	Univariate	38/152
Yahoo DatasetSyn ₁	0.83	1431	No	Unimodal	Weibull	Univariate	20/60
Yahoo DatasetSyn ₂	1.22	1472	No	Unimodal	Gamma	Univariate	30/90
Yahoo DatasetSyn ₃	1.24	1450	No	Unimodal	Weibull	Univariate	10/120
Yahoo DatasetSyn ₄	0.977	1432	No	Bimodal	Weibull	Univariate	105/210
Yahoo DatasetSyn ₅	1.32	1431	No	Bimodal	Weibull	Univariate	24/72
Yahoo DatasetSyn ₆	0.97	1431	No	Multimodal	Weibull	Univariate	74/148
Yahoo DatasetSyn ₇	1.12	1690	No	Unimodal	Weibull	Univariate	125/250
Yahoo DatasetSyn ₈	1.18	1690	No	Multimodal	Log-normal	Univariate	116/232
Yahoo DatasetSyn ₉	1.065	1690	No	Bimodal	Weibull	Univariate	30/90
Private synthetic industrial data							
GE DatasetSyn ₁	0.80	1619	No	Unimodal	Log-normal	Univariate	117/232
GE DatasetSyn ₂	3.30	554	No	Multimodal	Exponential	Univariate	50/150

Table 11: Anomaly Dataset Properties.

Appendix F VLDB

Using the VLDB Benchmark, we generated a timeseries dataset of 5500 datapoints containing 40 anomalies. We used various Deep Learning based algorithms on this generated non-industrial dataset. From table 12, we can clearly see that in terms of recall our proposed algorithm(Median-LSTM) works almost as well as GAN and far better than the other two. While in terms of precision Median-LSTM gives the best values, thus performing better than the other algorithms overall.

VLDB Dataset	Precision	Recall
Median-LSTM	0.513	0.976
GAN	0.0072	1
Autoencoders	0.013	0.025
Devnet	0.0357	0.158

Table 12: Comparison of Precision and Recall score for VLDB generated dataset for various deep learning anomaly detection techniques.